

DeAR: Fine-Grained VLM Adaptation by Decomposing Attention Head Roles

Yiming Ma^{1,*} Hongkun Yang^{2,*} Lionel Z. Wang^{3,†} Bin Chen^{1,4,†} Weizhi Xian¹ Jianzhi Teng³
¹Chongqing Research Institute of Harbin Institute of Technology, China
²Ocean University of China, China
³The Hong Kong Polytechnic University, Hong Kong SAR
⁴Harbin Institute of Technology (Shenzhen), China

Abstract

Prompt learning is a dominant paradigm for adapting pre-trained Vision-Language Models (VLMs) to downstream tasks. However, existing methods often rely on a simplistic, layer-centric view, assuming shallow layers capture general features while deep layers handle task-specific knowledge. This assumption results in uncontrolled interactions between learnable tokens and original tokens. Task-specific knowledge could degrade the model’s core generalization and creates a trade-off between task adaptation and the preservation of zero-shot generalization. To address this, we challenge the layer-centric view and propose **DeAR**, a framework that achieves fine-grained VLM adaptation by **Decomposing Attention head Roles**. We posit that the functional specialization within VLMs occurs not between layers, but at the finer-grained level of individual attention heads in the deeper layers. Based on this insight, we introduce a novel metric, *Concept Entropy*, to systematically classify attention heads into distinct functional roles: *Attribute*, *Generalization*, and *Mixed*. Guided by these roles, we introduce specialized attribute tokens and a *Role-Based Attention Mask* mechanism to precisely control information flow, ensuring generalization heads remain isolated from task-specific knowledge. We further incorporate a *Task-Adaptive Fusion Strategy* for inference. Extensive experiments on fifteen datasets show that DeAR achieves a strong balance between task adaptation and generalization, outperforming previous methods across various tasks. Our code is available at <https://github.com/wellsssssss/DeAR>

1. Introduction

Pre-trained Vision-Language Models (VLMs), such as CLIP [32], have emerged as a new paradigm in computer vision, demonstrating remarkable zero-shot generalization

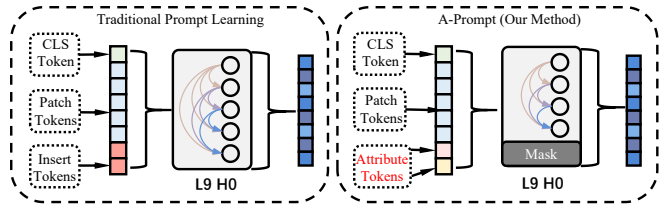


Figure 1. For a Generalization Head (e.g., Layer 9 Head 0), our Role-Based Mask explicitly blocking the original CLS and Patch tokens from interacting to the inserted Attribute Tokens.

capabilities across a wide range of downstream tasks. By leveraging contrastive learning on over 400 million image-text pairs, CLIP learns to align visual and textual inputs in a shared embedding space. This has led to impressive achievements in tasks such as text-image retrieval [32], visual question answering (VQA) [7], and open-vocabulary detection and segmentation [8, 41]. Moreover, the impact of CLIP extends to traditional vision tasks, such as image classification and object detection [22], where its zero-shot performance can surpass that of fully supervised methods.

Despite these successes, adapting CLIP to specific downstream tasks remains a significant challenge. Its pre-trained knowledge often lacks the granularity required for specialized domains. Although full fine-tuning could incorporate this new knowledge, it is computationally expensive and often leads to “catastrophic forgetting,” where the model loses its powerful zero-shot generalization abilities [20]. Consequently, Parameter-Efficient Fine-Tuning (PEFT) methods have become the mainstream approach [26, 42]. These methods keep the VLM backbone frozen and introduce a small number of trainable parameters. PEFT strategies include adapter-based methods and prompt learning. The former typically insert lightweight MLP layers to refine the output features [7, 36, 52], while prompt learning has emerged as a dominant and effective paradigm.

Prompt learning for VLMs was pioneered by CoOp [49], which introduced “soft prompts”, learnable continuous

*Equal contribution. †Corresponding authors.

vectors, into the text encoder to adapt to downstream tasks. Subsequent work extended this concept to the vision domain, with VPT [17] demonstrating the effectiveness of visual prompting. A key breakthrough came with MaPLe [18], which proposed the first multi-modal prompt learning framework, tuning prompts in both the vision and text encoders and proving its superiority over uni-modal approaches.

However, even with a frozen backbone, prompt learning methods still risk losing generalization capabilities. Due to the nature of the Vision Transformer [4, 38], inserted tokens inevitably interact with original tokens via multi-head self-attention, which can harm generalization. Existing solutions attempt to address this by carefully selecting which layers to inject prompts into—some targeting early layers (MaPLe), while others target deeper ones (MMRL). These conflicting, layer-based strategies reveal a fundamental gap: they treat entire Transformer layers as black boxes, ignoring the diverse functional roles played by individual attention heads within them. This lack of a fine-grained, principled approach for integrating new knowledge results in the challenging trade-off between achieving effective adaptation and maintaining generalization.

To address these challenges, we draw inspiration from recent work on VLM interpretability [6] and propose a novel framework: **DeAR**, a novel framework for fine-grained VLM adaptation achieved by **Decomposing Attention head Roles**. Given that CLIP’s final image representation is constructed by its late attention layers, we suppose that the key to effective task adaptation, while preserving generalization, is to focus on the functional specialization of these individual heads. Our approach begins by quantitatively analyzing the function of each attention head in the later layers of a ViT-B-16 backbone [4]. Using our proposed Concept Entropy metric, we classify these heads into distinct functional roles: Attribute Heads, Generalization Heads, and Mixed Heads. Leveraging this functional classification, DeAR introduces specialized, learnable attribute tokens and employs a role-based Attention Mask strategy. This mechanism precisely controls the information flow, guiding attribute tokens to interact primarily with their corresponding expert heads, while critically isolating the generalization heads from any new task-specific knowledge (Figure 1). Our contributions are as follows:

- We introduce **Concept Entropy**, a novel quantitative metric to systematically analyze and classify the functional roles of attention heads in ViT-B/16, revealing a clear specialization into Attribute, Generalization, and Mixed roles.
- We propose the **DeAR**, which introduces a Role-Based Attention Mask to leverage this functional map. This mechanism achieves controllable fine-tuning by precisely routing new knowledge to expert heads while shielding

generalization heads, achieving a balance between task-specific adaptation and the preservation of generalization capabilities.

- We demonstrate through extensive experiments that DeAR achieves **new state-of-the-art performance** on the challenging base-to-novel generalization benchmark.

2. Related Work

2.1. Vision-Language Models (VLMs)

Foundational Vision-Language Models (VLMs) have revolutionized multimodal learning. This paradigm was pioneered by CLIP [32], which established a powerful contrastive learning framework on massive web-scale data. Subsequent efforts have expanded on this foundation in diverse ways: ALIGN [16] demonstrated the power of training on even larger, noisier datasets; Florence [46] aimed for a universal visual representation via multi-task pre-training; SigLIP [47] enhanced scalability with a simpler pairwise sigmoid loss; and more recently, OpenVision [23] has proposed full transparency by leveraging high-quality, LLM-generated synthetic captions.

2.2. Prompt Learning for VLMs

Prompt learning has emerged as a dominant parameter-efficient strategy for adapting VLMs. The line of research was pioneered by CoOp, which replaces hand-crafted templates with learnable prompt vectors[49]. However, CoOp learns a single static prompt for the entire dataset, which tends to overfit seen classes and lacks adaptability to individual images. Subsequent studies proposed CoCoOp, which conditions prompts on each image, and Task-Aware Clustering, which learns cluster-specific prompts for semantic subgroups[12, 50]. To preserve the general knowledge of the backbone, PromptSRC, ProGrad and TCP introduce various regularization techniques[11, 19, 51].

As research matured, the focus expanded from uni-modal text prompts toward multimodal strategies. MaPLe presents a framework for simultaneous prompting in both vision and language branches[18], and more recent work such as MMRL designs shared representation spaces to facilitate deeper cross-modal interactions[9]. The latest trend pursues fine-grained semantics: LLaMP employs LLMs as adaptive prompt learners, ATPrompt constructs hybrid attribute–category prompt structures, PromptKD exploits prompts for knowledge distillation, and TextRefiner mines internal visual knowledge of VLMs to refine prompts without external models[24, 25, 45, 48]. Alternatively, Skip Tuning forgoes additional parameters altogether and instead modifies the full fine-tuning baseline with layer-wise and class-wise skipping to improve knowledge transfer [43].

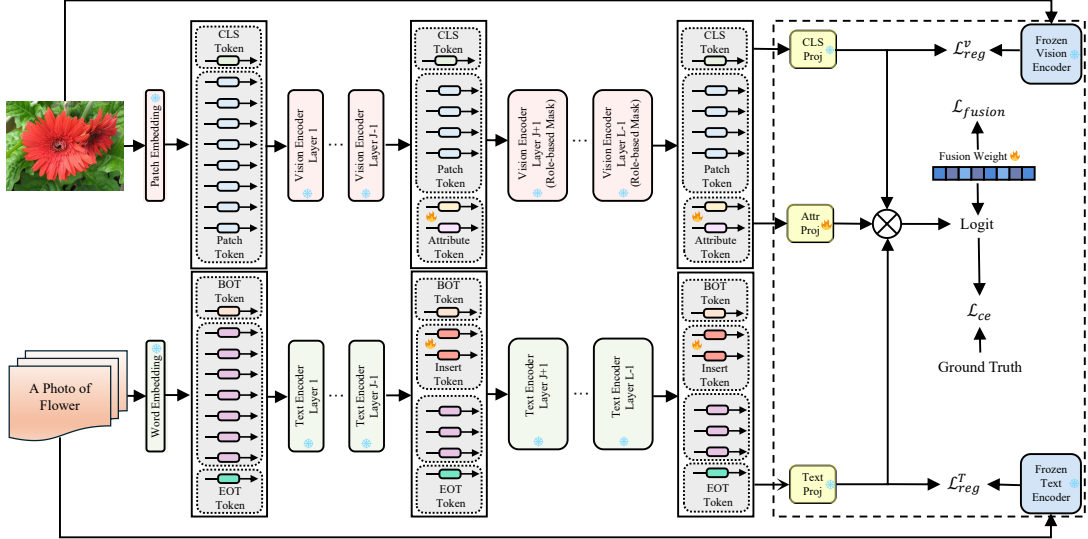


Figure 2. The overall framework of DeAR. At a deep layer J , we insert learnable attribute tokens into the frozen vision encoder and the text encoder. Information flow in these subsequent layers is precisely controlled by our Role-Based Attention Mask mechanism. For inference, the class feature (from the [CLS] token) and attribute feature first compute the logits with the text feature. These logits are then combined via learnable fusion weights to produce the final prediction.

3. Method

Despite advances in VLMs and prompt learning, efficiently adapting these models while maintaining generalization is still challenging. Most existing methods focus on designing representation spaces or using prompts to inject external knowledge, but rarely explore how internal information flows within the model. Our work, DeAR, addresses this by directly investigating these internal interactions to enable attribute-aware and interpretable prompt learning.

3.1. Revisiting the Vision Transformer

The ViT-based image encoder first converts an image into a sequence of patch embeddings. An input image \mathbf{x} is divided into N patches, which are linearly projected into D -dimensional vectors. A learnable [CLS] token, \mathbf{z}_{cls} , is prepended to this sequence, and position embeddings \mathbf{E}_{pos} are added to yield the initial token sequence $\mathbf{z}^0 \in \mathbb{R}^{(N+1) \times D}$.

This sequence is then processed by a stack of L Transformer layers. Each layer consists of a Multi-Head Self-Attention (MSA) module and a feed-forward MLP, with residual connections and layer normalization. Central to our work, the MSA mechanism allows tokens to interact through h parallel "attention heads." The MSA module's output is computed by concatenating the outputs of all heads, i.e., $\text{MSA}(\mathbf{z}) = \text{Concat}(\text{head}_1, \dots, \text{head}_h)\mathbf{W}_o$, where \mathbf{W}_o is a final projection layer. Each individual head

is computed via scaled dot-product attention:

$$\text{head}_i = \text{softmax} \left(\frac{\mathbf{Q}_i \mathbf{K}_i^T}{\sqrt{D_h}} \right) \mathbf{V}_i \quad (1)$$

The Query (\mathbf{Q}_i), Key (\mathbf{K}_i), and Value (\mathbf{V}_i) matrices for each head i are learned linear projections of the input tokens \mathbf{z} using per-head weight matrices ($\mathbf{W}_{q_i}, \mathbf{W}_{k_i}, \mathbf{W}_{v_i}$). After passing through all L layers, the final state of the class token, $\mathbf{z}_{\text{cls}}^L$, is projected to yield the final image feature \mathbf{f}_{cls} . This multi-head self-attention mechanism forms the foundation of our controllable fine-tuning framework.

3.2. Identifying Functional Roles of Attention Heads

The core of DeAR is our hypothesis, inspired by recent interpretability studies [6], that the functional specialization of a VLM resides not at the layer level, but within individual attention heads in the model's deeper layers [33]. We propose a novel, unsupervised methodology to first *identify* and then *quantify* the functional roles of these heads [39]. Our analysis focuses on the later layers (9–12) of ViT-B-16, which are known to be critical for constructing the final image representation.

To avoid subjective, pre-defined attribute categories, we adopt an approach to automatically identify conceptual clusters from the heads' description. Following Gandelsman et al. [6], we first use TEXTSPAN to generate a ranked list of top- N descriptive text phrases for each attention head. This yields a rich corpus of phrases describing each head's attentional focus. We then employ a pre-

Table 1. Representative examples of functionally specialized Attribute Heads identified in the later layers of ViT-B-16. Each head demonstrates a strong and unambiguous focus on a single core visual attribute, as evidenced by its top descriptive phrases.

Object Head (L12, H7)	Shape Head (L12, H5)	Texture Head (L11, H5)	Color Head (L12, H10)	Location Head (L12, H0)
- A stick	- A regular octagon	- Delicate embroidery	- An image with cold green tones	- Picture taken in Scotland
- A cup	- Rectangular object	- Intricate architectural carving	- Image with a red color	- Photo taken in Barcelona
- A bonnet	- A wavy pattern	- Artwork with kaleidoscopic patterns	- A charcoal gray color	- Photo taken in Tokyo, Japan
- A trampoline	- Herringbone pattern	- Image with woven basket textures	- Image with a yellow color	- Image taken in South Africa
- A shoelace	- A scalene triangle	- Artwork with Mondrian-like grids	- Image with a blue color	- Picture taken in Texas, USA
- A bottle	- A polka dot	- Image with calligraphy writing	- A platinum silver color	- Photo taken in Paris, France

trained SBERT, $S(\cdot)$ [35], to map each phrase into a high-dimensional semantic space. Instead of classifying these phrase embeddings into a fixed set of categories, we perform density-based clustering using HDBSCAN [29], a robust algorithm that can discover clusters of varying shapes and densities without requiring a pre-specified number of clusters. This automated process reveals a diverse set of conceptual clusters directly from the data.

Our clustering analysis revealed 12 distinct conceptual groups, including concepts such as *location*, *text*, *object*, *animal*, *photographic style*, and *emotion*, etc. From these, we selected five frequent and semantically orthogonal concepts most relevant for general visual recognition tasks: $A = \{\text{color, shape, texture, object, location}\}$. This process provides the conceptual basis for our subsequent analysis, where the centroid of each selected cluster c_j is denoted by its embedding $\bar{s}_j = S(c_j)$.

Quantifying Specialization with Concept Entropy.

With the core attributes established, we introduce a novel metric, **Concept Entropy**, to quantify the degree of functional specialization for each attention head (l, h) . For its top- N descriptive phrases $D_{(l,h)}$, we first classify each phrase d_i to the closest attribute cluster $c_j \in C$. This yields a probability distribution $P_{(l,h)}$ over the attributes, where $P_{(l,h)}(c_j)$ is the fraction of phrases assigned to c_j . Finally, the Concept Entropy $H(P_{(l,h)})$ is the Shannon entropy of this distribution. These steps are defined as:

$$\text{cat}(d_i) = \arg \max_{c_j \in C} \cos(S(d_i), \bar{s}_j) \quad (2)$$

$$P_{(l,h)}(c_j) = \frac{1}{N} \sum_{i=1}^N \mathbb{I}(\text{cat}(d_i) = c_j) \quad (3)$$

$$H(P_{(l,h)}) = - \sum_{j=1}^k P_{(l,h)}(c_j) \log_2 P_{(l,h)}(c_j) \quad (4)$$

where $\mathbb{I}(\cdot)$ is the indicator function. A low Concept Entropy score signifies that a head is highly specialized, concentrating its function on a single core attribute (**Attribute Head**). Conversely, a high score indicates a generalist function, engaging with a wide range of abstract concepts (**Generalization Head**). Heads with intermediate scores are classified as **Mixed Heads**. This role identification

framework forms the foundation for DeAR’s controllable learning mechanism.

3.3. DeAR: Fine-Grained Attribute-Aware Prompt Learning

Building on our function analysis of attention heads, we introduce DeAR, a framework consisting of three key components: multimodal attribute-aware prompt learning, a role-based attention mask mechanism, and a task-adaptive inference strategy. The overall framework is shown in Figure 2.

3.3.1. Multimodal Attribute-Aware Prompting

To adapt CLIP for downstream tasks, DeAR introduces learnable tokens into both the vision and text encoders, ensuring new knowledge is aligned across modalities.

Vision-Side Prompting. We initialize a set of learnable “attribute tokens,” $\{\mathbf{r}_{\text{attr}} \in \mathbb{R}^{D_v}\}_{\text{attr} \in A}$, where D_v is the feature dimension of the vision encoder. Here, A is the set of core visual attributes identified in our analysis, specifically $A = \{\text{color, shape, texture, object, location}\}$. Based on the findings of Gandelsman et al. [6] that the final image representation in CLIP is predominantly constructed by the later attention layers, these attribute tokens are integrated into the higher layers of the image encoder \mathcal{V} , beginning from the J -th layer (we set $J = 9$ in our experiments, following prior work on ViT analysis).

For the image encoder \mathcal{V} , the forward pass through the first $J - 1$ layers proceeds as standard:

$$[\mathbf{z}_{\text{cls}}^\ell, \mathbf{z}_p^\ell] = \mathcal{V}_\ell([\mathbf{z}_{\text{cls}}^{\ell-1}, \mathbf{z}_p^{\ell-1}]) \quad \ell = 1, \dots, J - 1$$

For subsequent layers $\ell \geq J$, the process involves the attribute tokens. Let $\mathbf{r}_{\text{attr}}^{\ell-1}$ be the state of an attribute token before entering layer ℓ . The Transformer layer \mathcal{V}_ℓ processes the augmented sequence to produce an updated, context-aware state $\tilde{\mathbf{r}}_{\text{attr}}^\ell$. The input to the *next* layer, $\mathbf{r}_{\text{attr}}^\ell$, is then determined by a controlled mixture:

$$\begin{aligned} [\mathbf{z}_{\text{cls}}^\ell, \mathbf{z}_p^\ell, \{\tilde{\mathbf{r}}_{\text{attr}}^\ell\}_{\text{attr} \in A}] &= \mathcal{V}_\ell([\mathbf{z}_{\text{cls}}^{\ell-1}, \mathbf{z}_p^{\ell-1}, \{\mathbf{r}_{\text{attr}}^{\ell-1}\}_{\text{attr} \in A}]) \\ [\mathbf{z}_{\text{cls}}^{\ell+1}, \mathbf{z}_p^{\ell+1}, \{\tilde{\mathbf{r}}_{\text{attr}}^{\ell+1}\}_{\text{attr} \in A}] & \\ &= \mathcal{V}_{\ell+1}([\mathbf{z}_{\text{cls}}^\ell, \mathbf{z}_p^\ell, \{\beta \mathbf{r}_{\text{attr}}^\ell + (1 - \beta) \tilde{\mathbf{r}}_{\text{attr}}^\ell\}_{\text{attr} \in A}]) \end{aligned} \quad (5)$$

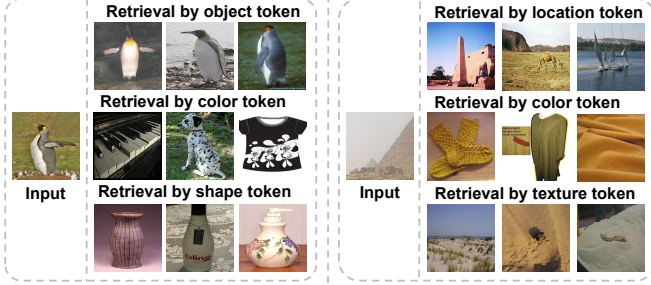


Figure 3. Results of attribute-conditioned image retrieval on ImageNet. For each query image, we retrieval using features from different learned attribute tokens.

Inspired by MMRL++ [10], we control the information flow between layers using the hyperparameter $\beta \in [0, 1]$. A purely sequential evolution ($\beta = 0$) allows tokens to adapt fully to the context of vision feature, but risks "semantic drift," where the token deviates from its core learned meaning. Conversely, a static re-injection of the raw token at each layer ($\beta = 1$) strongly preserves the core meaning but prevents any contextual adaptation. Our approach Eq. (5) strikes a flexible balance: it allows the attribute token to absorb image-specific information via $\tilde{\mathbf{r}}_{\text{attr}}^\ell$ while being regularized by its foundational prior \mathbf{r}_{attr} . This prevents the representation from deviating excessively from its core attribute meaning, leading to more stable prompt learning.

Text-Side Prompting. To ensure cross-modal alignment, we apply a symmetrical strategy to the text encoder \mathcal{W} . We initialize a set of K learnable tokens, $\{\mathbf{p}_k\}$, which are injected from layer J to L between the [BOT] and word tokens. Since text prompts for classification are typically simple templates (e.g., "a photo of {cls}"), a small set of parameters suffices for alignment without needing attribute-specific designs. The forward pass through the text encoder is then modified. For any given layer ℓ , let the full sequence of input tokens be $\mathbf{T}^{\ell-1}$. The output is computed as $\mathbf{T}^\ell = \mathcal{W}_\ell(\mathbf{T}^{\ell-1})$, where the prompt tokens within $\mathbf{T}^{\ell-1}$ are defined conditionally:

$$\mathbf{p}_k^{\text{in},\ell} = \begin{cases} \mathbf{p}_k^{\ell-1} & \text{if } \ell < J \\ \beta \mathbf{p}_k + (1 - \beta) \tilde{\mathbf{p}}_k^{\ell-1} & \text{if } \ell \geq J \end{cases} \quad (6)$$

Here, $\mathbf{p}_k^{\text{in},\ell}$ is the input prompt for layer ℓ , $\tilde{\mathbf{p}}_k^{\ell-1}$ is the context-aware output from the previous layer, and \mathbf{p}_k is the initial raw token. This controlled mixture, governed by β , allows contextual adaptation while preventing semantic drift. At inference, only the final [EOT] feature is used.

3.3.2. Role-Based Attention Mask

Preserving generalization requires precise control over the information flow between the original and newly introduced

attribute tokens. Building on our data-driven identification of head roles, we introduce a **role-based attention mask** mechanism. This mechanism, applied within the deeper layers of the ViT ($l \geq J$), assigns a custom attention mask $\mathbf{M}_{(l,h)} \in \{-\infty, 0\}^{N_{\text{seq}} \times N_{\text{seq}}}$ to each head (l, h) based on its specific function. The mask is applied additively to the raw attention scores:

$$\mathbf{S}_{(l,h)} = \frac{\mathbf{Q}_{(l,h)} \mathbf{K}_{(l,h)}^T}{\sqrt{D_h}} + \mathbf{M}_{(l,h)} \quad (7)$$

An entry $\mathbf{M}_{(l,h)}[i, j] = -\infty$ effectively severs the connection from query token i to key token j by setting its corresponding attention weight to zero post-softmax.

To formally define the masks, we partition the token indices into disjoint sets: \mathcal{I}_{cls} for the [CLS] token, $\mathcal{I}_{\text{patch}}$ for patch tokens, and $\mathcal{I}_{\text{attr}}$ for our learnable attribute tokens. The set of original token indices is $\mathcal{I}_{\text{orig}} = \mathcal{I}_{\text{cls}} \cup \mathcal{I}_{\text{patch}}$. The mask construction depends on the head's role:

Generalization and Other Specialized Heads. This category includes both **Generalization Heads**, and other **Specialized Heads** not selected as core attributes (e.g., for 'numbers' or 'text'). We hypothesize that both types of heads encode the model's intrinsic, pre-trained capabilities that are crucial for zero-shot generalization. To protect these foundational abilities from being perturbed by task-specific information, we implement a strict mask. This mask prohibits any interaction between the original tokens and our five learnable attribute tokens:

$$\mathbf{M}_{(l,h)}[i, j] = \begin{cases} -\infty & \text{if } (i \in \mathcal{I}_{\text{orig}} \text{ and } j \in \mathcal{I}_{\text{attr}}) \\ & \text{or } (i \in \mathcal{I}_{\text{attr}} \text{ and } j \in \mathcal{I}_{\text{orig}}) \\ 0 & \text{otherwise} \end{cases} \quad (8)$$

This policy ensures that both generalist heads and other specialist heads remain isolated, preserving their original functions.

Core Attribute Heads. These are the heads identified as specializing in one of our five core visual attributes $a \in A$ (e.g., 'color'). The mask for such a head is designed to channel the corresponding learnable attribute token exclusively to its expert head, enabling focused learning. Let $\mathcal{I}_{\text{attr}(a)} \subset \mathcal{I}_{\text{attr}}$ be the index set for the token(s) corresponding to attribute a . The mask is defined as:

$$\mathbf{M}_{(l,h)}[i, j] = \begin{cases} -\infty & \text{if } j \in \mathcal{I}_{\text{attr}} \text{ and } j \notin \mathcal{I}_{\text{attr}(a)} \\ 0 & \text{otherwise} \end{cases} \quad (9)$$

This rule allows any query token to attend to all original tokens and its relevant attribute token, while blocking attention to irrelevant ones. This promotes clean, disentangled attribute learning.

Mixed Heads. Heads with intermediate Concept Entropy are classified as **Mixed Heads**. We consider their function to be multifaceted and flexible. Therefore, we permit unrestricted attention by applying an all-zeros mask where $\mathbf{M}_{(l,h)}[i,j] = 0, \forall i, j$, allowing them to integrate information freely from all available tokens.

3.3.3. Final Feature Generation.

After passing through all L layers, the final hidden states of the [CLS] and attribute tokens are projected to generate features. The state of the original class token, $\mathbf{z}_{\text{cls}}^L$, is projected by the pre-trained and **frozen** vision projection head, $\mathbf{P}_{\text{vision}}(\cdot)$, to yield the class feature \mathbf{f}_{cls} :

$$\mathbf{f}_{\text{cls}} = \mathbf{P}_{\text{vision}}(\text{LN}(\mathbf{z}_{\text{cls}}^L)) \quad (10)$$

Similarly, the final state of each attribute token, $\mathbf{r}_{\text{attr}}^L$, is processed by a shared, **trainable** projection head, $\mathbf{P}_{\text{attr}}(\cdot)$, to yield a set of specialized attribute features $\{\mathbf{f}_{\text{attr}}\}$:

$$\mathbf{f}_{\text{attr}} = \mathbf{P}_{\text{attr}}(\text{LN}(\mathbf{r}_{\text{attr}}^L)) \quad (11)$$

This process yields a primary feature \mathbf{f}_{cls} retaining generalization, and specialized features \mathbf{f}_{attr} .

To visually validate our attribute tokens capture semantic concepts, we conduct an attribute-conditioned image retrieval, shown in Figure 3.

3.3.4. Training and Inference

Training. DeAR’s training process balances classification accuracy on the target task with preserving the model’s pre-trained generalization. The total loss function is a weighted combination of a primary classification loss and two regularization terms:

$$\mathcal{L}_{\text{total}} = \mathcal{L}_{\text{CE}} + \lambda_{\text{reg}} \mathcal{L}_{\text{reg}} + \lambda_{\text{fusion}} \mathcal{L}_{\text{fusion}} \quad (12)$$

where λ_{reg} and λ_{fusion} are hyperparameters that balance the contribution of each component.

The primary loss, $\mathcal{L}_{\text{CE}}(\hat{\mathbf{y}}, \mathbf{y})$, is the standard cross-entropy between the predicted logits $\hat{\mathbf{y}}$ (defined in our inference strategy [28], Eq. 19) and the ground-truth labels \mathbf{y} .

To preserve the model’s foundational knowledge, we introduce a self-regularization loss, \mathcal{L}_{reg} . This term encourages the final features from both the vision and text encoders to remain close to their counterparts from the original, frozen CLIP model. Specifically, we regularize the final class feature \mathbf{f}_{cls} and the text feature \mathbf{f}_t :

$$\mathcal{L}_{\text{reg}} = \mathcal{L}_{\text{reg}}^V + \mathcal{L}_{\text{reg}}^T \quad (13)$$

$$\mathcal{L}_{\text{reg}}^V = 1 - \cos(\mathbf{f}_{\text{cls}}, \mathbf{f}_{\text{cls}}^{\text{orig}}) \quad (14)$$

$$\mathcal{L}_{\text{reg}}^T = 1 - \cos(\mathbf{f}_t, \mathbf{f}_t^{\text{orig}}) \quad (15)$$

Here, $\mathbf{f}_{\text{cls}}^{\text{orig}}$ and $\mathbf{f}_t^{\text{orig}}$ are the features extracted from the unmodified CLIP model, and $\cos(\cdot, \cdot)$ denotes the cosine similarity.

To prevent over-reliance on the newly learned attribute features, we introduce a fusion-weight regularization, $\mathcal{L}_{\text{fusion}}$. This loss encourages the inference mechanism to assign a higher weight to the more general class feature:

$$\mathcal{L}_{\text{fusion}} = -\log(\alpha_{\text{cls}}) \quad (16)$$

where α_{cls} is the softmax-normalized weight corresponding to the class feature.

Task-Adaptive Fusion for Inference. For inference, we propose a **Task-Adaptive Fusion** strategy that combines evidence from the protected class and specialized attribute features. We learn a small set of scalar weights, $\{w_k\}_{k \in \{\text{cls}\} \cup \mathcal{A}}$, on the base classes, which are then fixed for novel classes.

For a given image and m class text embeddings $\{\mathbf{t}_j\}_{j=1}^m$, we first compute similarity vectors for the class feature \mathbf{f}_{cls} and each attribute feature \mathbf{f}_a :

$$\mathbf{s}_{\text{cls}} = \tau \cdot [\text{sim}(\mathbf{f}_{\text{cls}}, \mathbf{t}_1), \dots, \text{sim}(\mathbf{f}_{\text{cls}}, \mathbf{t}_m)] \quad (17)$$

$$\mathbf{s}_a = \tau \cdot [\text{sim}(\mathbf{f}_a, \mathbf{t}_1), \dots, \text{sim}(\mathbf{f}_a, \mathbf{t}_m)] \quad (18)$$

where τ is CLIP’s frozen temperature parameter. The final logits $\hat{\mathbf{y}}$ are a weighted sum of these vectors. The fusion weights α_k are derived from the learned scalars $\{w_k\}$ via softmax, where $\alpha_k = e^{w_k} / (e^{w_{\text{cls}}} + \sum_{i \in \mathcal{A}} e^{w_i})$. The final logits are then computed as:

$$\hat{\mathbf{y}} = \alpha_{\text{cls}} \cdot \mathbf{s}_{\text{cls}} + \sum_{a \in \mathcal{A}} \alpha_a \cdot \mathbf{s}_a. \quad (19)$$

This strategy assumes that a model’s reliance on specific attributes is a task-level prior (e.g., color is important for bird classification). By learning and transferring these priors, we achieve a more principled and effective fusion.

4. Experiments

4.1. Experiment settings

Implementation Details. Our implementation is based on the OpenCLIP with a ViT-B-16 backbone. We train the model using the AdamW optimizer with an initial learning rate of 1×10^{-3} . All experiments are conducted on three NVIDIA RTX 4090 GPUs. Further details are provided in the Appendix.

Base-to-Novel Generalization. This is the primary evaluation to assess DeAR’s ability to adapt to downstream tasks while preserving generalization. We conduct this evaluation across eleven image classification datasets: ImageNet [3], Caltech101 [5], OxfordPets [31], StanfordCars

Table 2. Comparison of DeAR with previous methods on base-to-novel generalization across 11 datasets. Bold values indicate the best results.

Method	Average			ImageNet			Caltech101			OxfordPets			StanfordCars			Flowers102		
	Base	Novel	HM															
CLIP (ICML2021)	69.34	74.22	71.70	72.43	68.14	70.22	96.84	94.00	95.40	91.17	97.96	94.12	63.37	74.89	68.65	72.08	77.80	74.83
CoOp (ICCV2021)	82.69	63.22	71.66	76.47	67.88	71.92	98.01	89.81	93.73	93.67	95.29	94.47	78.12	60.40	68.13	97.60	59.67	74.06
ATPrompt _{C_oOp} (ICCV2025)	82.68	68.04	74.65	76.27	70.60	73.33	97.95	93.63	95.74	94.77	96.59	95.67	77.43	66.55	71.58	97.44	67.52	79.77
ProGrad (CVPR2023)	82.48	70.75	76.16	77.02	66.66	71.46	98.02	93.89	95.91	95.07	97.63	96.33	77.68	68.63	72.88	95.54	71.87	82.03
MaPLe (CVPR2023)	82.28	75.14	78.55	76.60	70.54	73.47	97.74	94.36	96.02	95.43	97.76	96.58	72.94	74.00	73.47	95.92	72.46	82.56
PromptSRC (ICCV2023)	84.26	76.10	79.97	77.60	70.73	74.01	98.10	94.03	96.02	95.33	97.30	96.30	78.27	74.97	76.58	98.07	76.50	85.95
ProVP (CVPR2024)	85.20	73.22	78.76	75.82	69.21	72.36	98.92	94.21	96.51	95.87	97.65	96.75	80.43	67.96	73.67	98.42	72.06	83.20
TCP (CVPR2024)	84.13	75.36	79.51	77.27	69.87	73.38	98.23	94.67	96.42	94.67	97.20	95.92	80.80	74.13	77.32	97.73	75.57	85.23
PromptKD (CVPR2024)	84.11	78.28	81.09	77.63	70.96	74.15	98.31	96.29	97.29	93.42	97.44	95.39	80.48	81.78	81.12	98.69	81.91	89.52
MMRL (CVPR2025)	85.68	77.16	81.20	77.90	71.30	74.45	98.97	94.50	96.68	95.90	97.60	96.74	81.30	75.07	78.06	98.97	77.27	86.78
TAC (CVPR2025)	85.24	77.60	81.24	78.57	71.03	74.61	98.57	95.27	96.89	95.93	98.17	97.04	81.63	74.17	77.72	97.97	76.87	86.15
SkipT (CVPR2025)	85.04	77.53	81.11	77.73	70.40	73.89	98.50	95.33	96.89	95.70	97.87	96.77	82.93	72.50	77.37	98.57	75.80	85.70
DeAR (Ours)	85.94	79.73	82.72	78.12	71.80	74.83	99.00	95.80	96.95	97.34	97.50	96.81	82.01	75.20	78.47	99.00	78.50	87.57

Method	Food101			FGVC Aircraft			SUN397			DTD			EuroSAT			UCF101		
	Base	Novel	HM	Base	Novel	HM	Base	Novel	HM	Base	Novel	HM	Base	Novel	HM	Base	Novel	HM
CLIP (ICML2021)	90.10	91.22	90.66	27.19	36.29	31.09	69.36	75.35	72.23	53.24	59.90	56.37	56.48	64.05	60.03	70.53	77.50	73.85
CoOp (ICCV2021)	88.33	82.26	85.19	40.44	22.30	28.75	80.60	65.89	72.51	79.44	41.18	54.24	92.19	54.74	68.69	84.69	56.05	67.46
ATPrompt _{C_oOp} (ICCV2025)	88.74	87.44	88.09	40.38	27.22	32.52	80.84	68.64	74.24	80.83	45.49	58.22	90.34	59.79	71.96	84.49	64.96	73.45
ProGrad (CVPR2023)	90.37	89.59	89.98	40.54	27.57	32.82	81.26	74.17	77.55	77.35	52.35	62.45	90.11	60.89	72.67	84.33	74.94	79.35
MaPLe (CVPR2023)	90.71	92.05	91.38	37.44	35.61	36.50	80.82	78.70	79.75	80.36	59.18	68.16	94.07	73.23	82.35	83.00	78.66	80.77
PromptSRC (ICCV2023)	90.67	91.53	91.10	42.73	37.87	40.15	82.67	78.47	80.52	83.37	62.97	71.75	92.90	73.90	82.32	87.10	78.80	82.74
ProVP (CVPR2024)	90.32	90.91	90.61	47.08	29.87	36.55	83.14	74.71	78.73	62.11	65.53	63.77	97.12	72.91	83.29	87.30	79.00	83.00
TCP (CVPR2024)	90.57	91.37	90.97	41.97	34.43	37.83	82.63	78.20	80.35	82.77	58.07	68.25	91.63	74.73	82.32	87.13	80.77	83.83
PromptKD (CVPR2024)	89.43	91.27	90.34	43.61	39.68	41.55	82.53	80.88	81.70	82.86	69.15	75.39	92.04	71.59	80.54	86.23	80.11	83.06
MMRL (CVPR2025)	90.57	91.50	91.03	46.30	37.03	41.15	83.20	79.30	81.20	85.67	65.00	73.82	95.60	80.17	87.21	88.10	80.07	83.89
TAC (CVPR2025)	90.87	91.87	91.37	44.60	37.70	40.86	83.70	80.03	81.82	83.37	64.27	72.58	94.37	82.60	88.10	88.07	81.67	84.75
SkipT (CVPR2025)	90.67	92.03	91.34	45.37	37.13	40.84	82.40	79.03	80.68	83.77	67.23	74.59	92.47	83.00	87.48	87.30	82.47	84.81
DeAR (Ours)	90.10	91.90	90.93	47.10	38.90	42.61	83.82	81.80	82.80	83.90	75.60	79.62	97.00	87.90	92.22	87.90	82.10	84.90

[21], Flowers102 [30], Food101 [1], FGVC Aircraft [27], SUN397 [44], UCF101 [37], DTD [2], and EuroSAT [13]. We follow the standard setup: the model trains on 16-shot base classes and is evaluated on the test sets of both base and novel classes. As shown in Table 2, DeAR demonstrates clear superiority, achieving a new state-of-the-art harmonic mean of 82.72%. This result is driven by a significant 1.83% improvement on novel classes over the previous best, MMRL. The substantial gain on unseen classes directly validates our core hypothesis: protecting generalization heads is crucial for preserving the model’s foundational knowledge.

Domain Generalization. This evaluation measures the model’s robustness to out-of-distribution data and domain shifts. Following standard practice, we train the model on the 16-shot ImageNet training set (all classes) and directly evaluate its performance, without further fine-tuning, on four challenging ImageNet variants: ImageNetV2 [34], ImageNet-Sketch [40], ImageNet-A [15], and ImageNet-R [14]. Table 4 presents the domain generalization results. Our method demonstrates consistently strong robustness across all four out-of-distribution datasets. DeAR achieves the best performance on ImageNet-A (51.80%) and ImageNet-R (78.83%), also is highly competitive in the other variants.

Few-Shot Learning. Few-shot learning evaluates the capacity of the model for knowledge transfer and generalization when labeled data are limited. To quantify this capability, we fine-tune DeAR on k shot subsets of the original training data, where $k \in \{1, 2, 4, 8, 16\}$. As shown in Figure 4, across all settings from 1 to 16 shots, DeAR consistently outperforms the baseline methods, demonstrating a slight but consistent performance advantage. This suggests that our DeAR framework provides robust performance even in limited labeled data. Detailed results on all 11 datasets are provided in the Appendix.

Cross-Dataset Generalization. To evaluate transfer ability, we train DeAR on ImageNet (16 shots per class) and test it zero-shot on ten unseen datasets. Since the Task-Adaptive Fusion weights are optimized for ImageNet, they may not generalize. Therefore, for a fair evaluation on the target datasets, we adopt a decoupled inference strategy similar to MMRL [9], using only the protected class feature \mathbf{f}_{cls} for prediction. As shown in Table 3, DeAR sets a new state-of-the-art average accuracy of 67.60%, surpassing the previous best method, MMRL, while maintaining comparable performance on the source task (ImageNet).

4.2. Ablation Studies

To validate the effectiveness of the key components in our DeAR framework, we conduct a series of ablation studies

Table 3. Comparison of DeAR with previous methods on cross-dataset evaluation. Bold values indicate the best results.

	Source	Target										
	ImageNet	Average	Caltech101	OxfordPets	StanfordCars	Flowers102	Food101	FGVC-Aircraft	SUN397	DTD	EuroSAT	UCF101
CoOp	71.51	63.88	93.70	89.14	64.51	68.71	85.30	18.47	64.15	41.92	46.39	66.55
MaPLe	70.72	66.30	93.53	90.49	65.57	72.23	86.20	24.74	67.01	46.49	48.06	68.69
PromptSRC	71.27	65.81	93.60	90.25	65.70	70.25	86.15	23.90	67.10	46.87	45.50	68.75
MMRL	72.03	67.25	94.67	91.43	66.10	72.77	86.40	26.30	67.57	45.90	53.10	68.27
TAC	72.77	66.53	94.53	90.67	65.30	72.20	85.83	23.53	67.63	47.57	48.07	70.00
DeAR (Ours)	71.50	67.60	95.00	91.23	66.70	73.80	86.80	26.50	68.30	45.40	53.50	68.80

Table 4. Comparison of DeAR with previous methods on domain generalization. Bold values indicate the best results.

	Source	Target				
	ImageNet	Average	-V2	-S	-A	-R
CoOp	71.51	59.28	64.20	47.99	49.71	75.21
MaPLe	70.72	60.28	64.07	49.15	50.90	76.98
PromptSRC	71.27	60.65	64.35	49.55	50.90	77.80
MMRL	72.03	60.59	64.47	49.17	51.20	77.53
TAC	72.77	61.63	65.97	50.30	51.73	78.50
DeAR (Ours)	71.50	61.25	64.87	49.50	51.80	78.83



Figure 4. Comparison of DeAR with previous methods on few-shot learning. Detailed results are provided in the Appendix

on the average performance across all 11 datasets in the base-to-novel generalization setting.

Role-Based Attention Mask. To validate our core hypothesis, that role-based information control is superior to uniform strategies, we compare DeAR against two variants: All-Generalization, where all deep heads are shielded from attribute tokens, and All-Mixed, where all interactions are permitted.

The results shown in Table 5 validate our role-based design. The All-Generalization strategy maximizes novel-class performance at the cost of base-class learning, while the All-Mixed strategy does the opposite. Our proposed DeAR strikes the optimal balance between adaptation and generalization, achieving the best overall Harmonic Mean.

Table 5. Ablation on Role-Based Attention Mask.

Mask Strategy	Base	Novel	HM
All-Generalization	81.25	80.12	80.68
All-Mixed	85.31	76.98	80.93
DeAR (Ours)	85.94	79.73	82.72

Impact of Loss Components. We also analyze the contribution of each component in our proposed loss function. We start with a baseline using only the cross-entropy classification loss (\mathcal{L}_{CE}) and incrementally add our two regularization terms: the multimodal self-regularization (\mathcal{L}_{reg}) and the fusion-weight regularization (\mathcal{L}_{fusion}).

As shown in Table 6, each loss component is vital. Adding \mathcal{L}_{reg} significantly boosts Novel class performance (+4.24%). The subsequent addition of \mathcal{L}_{fusion} further improves the overall Harmonic Mean, demonstrating the benefit of prioritizing the class feature.

Table 6. Ablation on Loss function components.

Loss Function	Base	Novel	HM
\mathcal{L}_{CE}	86.75	74.21	79.99
$\mathcal{L}_{CE} + \mathcal{L}_{reg}$	85.03	78.45	81.61
$\mathcal{L}_{CE} + \mathcal{L}_{reg} + \mathcal{L}_{fusion}$	85.94	79.73	82.72

5. Conclusion

In this work, we propose the DeAR framework to enhance the adaptation of CLIP by balancing task-specific knowledge with generalization preservation. DeAR offers a fine-grained controllable fine-tuning process. Using our Concept Entropy, we decompose each attention head roles, allowing DeAR to direct new knowledge to attribute heads while protecting generalization heads. Experiments show that DeAR achieves state-of-the-art performance on base-to-novel generalization benchmarks and performs well on various tasks. More importantly, the learned attribute-aware representations offer significant potential for future applications requiring explicit semantic control, such as fine-grained retrieval. We demonstrate that fine-grained internal control is the path to better VLMs adaptation.

References

- [1] Lukas Bossard, Matthieu Guillaumin, and Luc Van Gool. Food-101 – mining discriminative components with random forests. In *Computer Vision – ECCV 2014*, pages 446–461, Cham, 2014. Springer International Publishing. 7
- [2] Mircea Cimpoi, Subhransu Maji, Iasonas Kokkinos, Sammy Mohamed, and Andrea Vedaldi. Describing textures in the wild. In *2014 IEEE Conference on Computer Vision and Pattern Recognition*, pages 3606–3613, 2014. 7
- [3] Jia Deng, Wei Dong, Richard Socher, Li-Jia Li, Kai Li, and Li Fei-Fei. Imagenet: A large-scale hierarchical image database. In *2009 IEEE Conference on Computer Vision and Pattern Recognition*, pages 248–255, 2009. 6
- [4] Alexey Dosovitskiy, Lucas Beyer, Alexander Kolesnikov, Dirk Weissenborn, Xiaohua Zhai, Thomas Unterthiner, Mostafa Dehghani, Matthias Minderer, Georg Heigold, Sylvain Gelly, Jakob Uszkoreit, and Neil Houlsby. An image is worth 16x16 words: Transformers for image recognition at scale, 2021. 2
- [5] Li Fei-Fei, R. Fergus, and P. Perona. Learning generative visual models from few training examples: An incremental bayesian approach tested on 101 object categories. In *2004 Conference on Computer Vision and Pattern Recognition Workshop*, pages 178–178, 2004. 6
- [6] Yossi Gandelsman, Alexei A. Efros, and Jacob Steinhardt. Interpreting CLIP’s image representation via text-based decomposition. In *The Twelfth International Conference on Learning Representations*, 2024. 2, 3, 4
- [7] Peng Gao, Shijie Geng, Renrui Zhang, Teli Ma, Rongyao Fang, Yongfeng Zhang, Hongsheng Li, and Yu Qiao. Clip-adapter: Better vision-language models with feature adapters, 2025. 1
- [8] Xiuye Gu, Tsung-Yi Lin, Weicheng Kuo, and Yin Cui. Open-vocabulary object detection via vision and language knowledge distillation, 2022. 1
- [9] Yuncheng Guo and Xiaodong Gu. Mmrl: Multi-modal representation learning for vision-language models. In *Proceedings of the Computer Vision and Pattern Recognition Conference*, pages 25015–25025, 2025. 2, 7
- [10] Yuncheng Guo and Xiaodong Gu. Mmrl++: Parameter-efficient and interaction-aware representation learning for vision-language models, 2025. 5
- [11] Changsheng Xu Hantao Yao, Rui Zhang. Tcpl: Textual-based class-aware prompt tuning for visual-language model. In *The IEEE/CVF Conference on Computer Vision and Pattern Recognition*, 2024. 2
- [12] Fusheng Hao, Fengxiang He, Fuxiang Wu, Tichao Wang, Chengqun Song, and Jun Cheng. Task-aware clustering for prompting vision-language models. In *Proceedings of the Computer Vision and Pattern Recognition Conference (CVPR)*, pages 14745–14755, 2025. 2
- [13] Patrick Helber, Benjamin Bischke, Andreas Dengel, and Damian Borth. Eurosat: A novel dataset and deep learning benchmark for land use and land cover classification. *IEEE Journal of Selected Topics in Applied Earth Observations and Remote Sensing*, 12(7):2217–2226, 2019. 7
- [14] Dan Hendrycks, Steven Basart, Norman Mu, Saurav Kadavath, Frank Wang, Evan Dorundo, Rahul Desai, Tyler Zhu, Samyak Parajuli, Mike Guo, Dawn Song, Jacob Steinhardt, and Justin Gilmer. The many faces of robustness: A critical analysis of out-of-distribution generalization. In *2021 IEEE/CVF International Conference on Computer Vision (ICCV)*, pages 8320–8329, 2021. 7
- [15] Dan Hendrycks, Kevin Zhao, Steven Basart, Jacob Steinhardt, and Dawn Song. Natural adversarial examples. In *2021 IEEE/CVF Conference on Computer Vision and Pattern Recognition (CVPR)*, pages 15257–15266, 2021. 7
- [16] Chao Jia, Yinfei Yang, Ye Xia, Yi-Ting Chen, Zarana Parekh, Hieu Pham, Quoc Le, Yun-Hsuan Sung, Zhen Li, and Tom Duerig. Scaling up visual and vision-language representation learning with noisy text supervision. In *Proceedings of the 38th International Conference on Machine Learning*, pages 4904–4916. PMLR, 2021. 2
- [17] Menglin Jia, Luming Tang, Bor-Chun Chen, Claire Cardie, Serge Belongie, Bharath Hariharan, and Ser-Nam Lim. Visual prompt tuning, 2022. 2
- [18] Muhammad Uzair khattak, Hanoona Rasheed, Muhammad Maaz, Salman Khan, and Fahad Shahbaz Khan. Maple: Multi-modal prompt learning. In *The IEEE/CVF Conference on Computer Vision and Pattern Recognition*, 2023. 2
- [19] Muhammad Uzair Khattak, Syed Talal Wasim, Muzammal Naseer, Salman Khan, Ming-Hsuan Yang, and Fahad Shahbaz Khan. Self-regulating prompts: Foundational model adaptation without forgetting. In *Proceedings of the IEEE/CVF International Conference on Computer Vision (ICCV)*, pages 15190–15200, 2023. 2
- [20] James Kirkpatrick, Razvan Pascanu, Neil Rabinowitz, Joel Veness, Guillaume Desjardins, Andrei A Rusu, Kieran Milan, John Quan, Tiago Ramalho, Agnieszka Grabska-Barwinska, et al. Overcoming catastrophic forgetting in neural networks. *Proceedings of the national academy of sciences*, 114(13):3521–3526, 2017. 1
- [21] Jonathan Krause, Michael Stark, Jia Deng, and Li Fei-Fei. 3d object representations for fine-grained categorization. In *2013 IEEE International Conference on Computer Vision Workshops*, pages 554–561, 2013. 7
- [22] Liunian Harold Li, Pengchuan Zhang, Haotian Zhang, Jianwei Yang, Chunyuan Li, Yiwu Zhong, Lijuan Wang, Lu Yuan, Lei Zhang, Jenq-Neng Hwang, Kai-Wei Chang, and Jianfeng Gao. Grounded language-image pre-training. In *2022 IEEE/CVF Conference on Computer Vision and Pattern Recognition (CVPR)*, pages 10955–10965, 2022. 1
- [23] Xianhang Li, Yanqing Liu, Haoqin Tu, Hongru Zhu, and Cihang Xie. Openvision: A fully-open, cost-effective family of advanced vision encoders for multimodal learning, 2025. 2
- [24] Zheng Li, Xiang Li, Xinyi Fu, Xin Zhang, Weiqiang Wang, Shuo Chen, and Jian Yang. Promptkd: Unsupervised prompt distillation for vision-language models. In *Proceedings of the IEEE/CVF Conference on Computer Vision and Pattern Recognition*, pages 26617–26626, 2024. 2
- [25] Zheng Li, Yibing Song, Ming-Ming Cheng, Xiang Li, and Jian Yang. Advancing textual prompt learning with anchored attributes. In *Proceedings of the IEEE/CVF International Conference on Computer Vision*, pages 3618–3627, 2025. 2

- [26] Nayu Liu, Junnan Zhu, Yiming Ma, Zhicong Lu, Wenlei Xu, Yong Yang, Jiang Zhong, and Kaiwen Wei. Sara: Saliency-aware reinforced adaptive decoding for large language models in abstractive summarization. In *Proceedings of the 63rd Annual Meeting of the Association for Computational Linguistics (Volume 1: Long Papers)*, pages 25450–25463, 2025. 1
- [27] Subhransu Maji, Esa Rahtu, Juho Kannala, Matthew Blaschko, and Andrea Vedaldi. Fine-grained visual classification of aircraft, 2013. 7
- [28] Anqi Mao, Mehryar Mohri, and Yutao Zhong. Cross-entropy loss functions: Theoretical analysis and applications, 2023. 6
- [29] Leland McInnes, John Healy, Steve Astels, et al. hdbscan: Hierarchical density based clustering. *J. Open Source Softw.*, 2(11):205, 2017. 4
- [30] Maria-Elena Nilsback and Andrew Zisserman. Automated flower classification over a large number of classes. In *2008 Sixth Indian Conference on Computer Vision, Graphics & Image Processing*, pages 722–729, 2008. 7
- [31] Omkar M Parkhi, Andrea Vedaldi, Andrew Zisserman, and C. V. Jawahar. Cats and dogs. In *2012 IEEE Conference on Computer Vision and Pattern Recognition*, pages 3498–3505, 2012. 6
- [32] Alec Radford, Jong Wook Kim, Chris Hallacy, Aditya Ramesh, Gabriel Goh, Sandhini Agarwal, Girish Sastry, Amanda Askell, Pamela Mishkin, Jack Clark, Gretchen Krueger, and Ilya Sutskever. Learning transferable visual models from natural language supervision, 2021. 1, 2
- [33] Maithra Raghu, Thomas Unterthiner, Simon Kornblith, Chiyuan Zhang, and Alexey Dosovitskiy. Do vision transformers see like convolutional neural networks? In *Proceedings of the 35th International Conference on Neural Information Processing Systems*, Red Hook, NY, USA, 2021. Curran Associates Inc. 3
- [34] Benjamin Recht, Rebecca Roelofs, Ludwig Schmidt, and Vaishal Shankar. Do imagenet classifiers generalize to imagenet? In *International Conference on Machine Learning*, 2019. 7
- [35] Nils Reimers and Iryna Gurevych. Sentence-BERT: Sentence embeddings using Siamese BERT-networks. In *Proceedings of the 2019 Conference on Empirical Methods in Natural Language Processing and the 9th International Joint Conference on Natural Language Processing (EMNLP-IJCNLP)*, pages 3982–3992, Hong Kong, China, 2019. Association for Computational Linguistics. 4
- [36] Dominykas Seputis, Serghei Mihailov, Soham Chatterjee, and Zehao Xiao. Multi-modal adapter for vision-language models, 2024. 1
- [37] Khurram Soomro, Amir Zamir, and Mubarak Shah. Ucf101: A dataset of 101 human actions classes from videos in the wild. *ArXiv*, abs/1212.0402, 2012. 7
- [38] Ashish Vaswani, Noam Shazeer, Niki Parmar, Jakob Uszkoreit, Llion Jones, Aidan N. Gomez, Lukasz Kaiser, and Illia Polosukhin. Attention is all you need, 2023. 2
- [39] Jesse Vig and Yonatan Belinkov. Analyzing the structure of attention in a transformer language model. In *Proceedings of the 2019 ACL Workshop BlackboxNLP: Analyzing and Interpreting Neural Networks for NLP*, pages 63–76, Florence, Italy, 2019. Association for Computational Linguistics. 3
- [40] Haohan Wang, Songwei Ge, Zachary Lipton, and Eric P Xing. Learning robust global representations by penalizing local predictive power. In *Advances in Neural Information Processing Systems*. Curran Associates, Inc., 2019. 7
- [41] Junjie Wang, Bin Chen, Bin Kang, Yulin Li, Weizhi Xian, Yichi Chen, and Yong Xu. Ov-dqo: Open-vocabulary detr with denoising text query training and open-world unknown objects supervision. *Proceedings of the AAAI Conference on Artificial Intelligence*, 39(7):7762–7770, 2025. 1
- [42] Lionel Z. Wang, Yiming Ma, Renfei Gao, Beichen Guo, Han Zhu, Wenqi Fan, Zexin Lu, and Ka Chung Ng. Megafake: A theory-driven dataset of fake news generated by large language models, 2024. 1
- [43] Shihan Wu, Ji Zhang, Pengpeng Zeng, Lianli Gao, Jingkuan Song, and Heng Tao Shen. Skip tuning: Pre-trained vision-language models are effective and efficient adapters themselves. *arXiv preprint arXiv:2412.11509*, 2024. 2
- [44] Jianxiong Xiao, James Hays, Krista A. Ehinger, Aude Oliva, and Antonio Torralba. Sun database: Large-scale scene recognition from abbey to zoo. In *2010 IEEE Computer Society Conference on Computer Vision and Pattern Recognition*, pages 3485–3492, 2010. 7
- [45] Jingjing Xie, Yuxin Zhang, Jun Peng, Zhaohong Huang, and Liujuan Cao. Textrefiner: Internal visual feature as efficient refiner for vision-language models prompt tuning, 2024. 2
- [46] Lu Yuan, Dongdong Chen, Yi-Ling Chen, Noel Codella, Xiyang Dai, Jianfeng Gao, Houdong Hu, Xuedong Huang, Boxin Li, Chunyuan Li, Ce Liu, Mengchen Liu, Zicheng Liu, Yumao Lu, Yu Shi, Lijuan Wang, Jianfeng Wang, Bin Xiao, Zhen Xiao, Jianwei Yang, Michael Zeng, Luwei Zhou, and Pengchuan Zhang. Florence: A new foundation model for computer vision, 2021. 2
- [47] Xiaohua Zhai, Basil Mustafa, Alexander Kolesnikov, and Lucas Beyer. Sigmoid loss for language image pre-training. In *2023 IEEE/CVF International Conference on Computer Vision (ICCV)*, pages 11941–11952, 2023. 2
- [48] Zhaoheng Zheng, Jingmin Wei, Xuefeng Hu, Haidong Zhu, and Ram Nevatia. Large language models are good prompt learners for low-shot image classification. In *CVPR*, 2024. 2
- [49] Kaiyang Zhou, Jingkang Yang, Chen Change Loy, and Ziwei Liu. Learning to prompt for vision-language models. *International Journal of Computer Vision*, 130(9):2337–2348, 2022. 1, 2
- [50] Kaiyang Zhou, Jingkang Yang, Chen Change Loy, and Ziwei Liu. Conditional prompt learning for vision-language models. In *IEEE/CVF Conference on Computer Vision and Pattern Recognition (CVPR)*, 2022. 2
- [51] Beier Zhu, Yulei Niu, Yucheng Han, Yue Wu, and Hanwang Zhang. Prompt-aligned gradient for prompt tuning. *International Conference on Computer Vision*, 2023. 2
- [52] Xiangyang Zhu, Renrui Zhang, Bowei He, Aojun Zhou, Dong Wang, Bin Zhao, and Peng Gao. Not all features matter: Enhancing few-shot clip with adaptive prior refinement, 2023. 1